CANCER BIOLOGY & THERAPY
2026, VOL. 27, NO. 1, 2684140
https://doi.org/10.1080/15384047.2026.2684140

Taylor & Francis
by informa

RESEARCH ARTICLE

OPEN ACCESS Check for updates

Neoplastic CD3⁺ B cells remodel the DLBCL tumor microenvironment via single-cell and spatial transcriptomics

Mingxiao Lang[a,1], Youqin Feng[a,1], Li Zhou[b], Bin Li[c], Wei Li[a], Jing Zhao[a], Kexin Chen[d], Lanfang Li[a], Lihua Qiu[a], Zhengzi Qian[a], Shiyong Zhou[a], Huilai Zhang[a] and Zhaobin Chu[e]

[a]National Clinical Research Center for Cancer, Tianjin's Clinical Research Center for Cancer, Key Laboratory of Cancer Prevention and Therapy, Department of Lymphoma, Tianjin Medical University Cancer Institute & Hospital, Tianjin, China; [b]Beijing Easyresearch Technology Limited, Beijing, China; [c]Department of Gastric Surgery, Tianjin Medical University Cancer Institute & Hospital, National Clinical Research Center for Cancer, Tianjin's Clinical Research Center for Cancer, Key Laboratory of Digestive Cancer, Tianjin, China; [d]Department of Joint Laboratory for Translational Medicine Research, Liaocheng People's Hospital, Liaocheng, China; [e]College of Life Sciences, University of Chinese Academy of Sciences, Beijing, China

ABSTRACT

Introduction: This study constructs a high-resolution multi-omics map of Diffuse Large B-Cell Lymphoma (DLBCL) by integrating single-cell, single-nucleus, and spatial transcriptomics.
Methods: We identified a previously unrecognized, recurrent subset of malignant B cells that unexpectedly express CD3, a protein typically found only on T cells. This unusual CD3⁺ B cell population appears to be driven by a specific genetic circuit involving five key regulatory genes: BCLAF1, CHURC1, FLI1, NFATC2, and ELF2.
Result: Spatial and functional analyses revealed that these cells are associated with macrophage enrichment and M2 polarization, potentially involving TGF-β signaling and contributing to an immunosuppressive tumor microenvironment. Clinically, the abundance of CD3⁺ B cells was associated with advanced disease stage, poor treatment response, and reduced survival.
Conclusion: Our findings support the presence of a CD3⁺ B cell subset with T cell-like features that is associated with tumor microenvironment remodeling and adverse clinical outcomes, highlighting molecular determinants like FLI1 and the TGF-β axis as potential therapeutic targets.

ARTICLE HISTORY
Received 3 February 2026
Revised 29 April 2026
Accepted 27 May 2026

KEYWORDS
Diffused large B-cell lymphoma; CD3 complex; tumor microenvironment; RNA sequencing; spatial transcriptomics

Introduction

Diffuse large B-cell lymphoma (DLBCL), the most common subtype of non-Hodgkin's lymphoma, is an aggressive and heterogeneous disease.[1] Although current frontline therapy—R-CHOP (rituximab plus cyclophosphamide, doxorubicin, vincristine, and prednisone)—achieves appreciable remission rates, it remains fatal in approximately 40% of patients due to unresolved mechanisms of treatment resistance.[2] Gene expression profiling has classified DLBCL into two major cell of origin (COO) subtypes,[3] with the germinal center B cell-like (GCB) subtype generally associated with better prognosis than the activated B cell-like (ABC) subtype. Moreover, recent studies have identified several molecular subtypes with distinct oncogenic pathways and genotypic alterations,[4,5] further emphasizing that neoplastic B cell heterogeneity contributes to divergent clinical outcomes. Thus, elucidating the basis of DLBCL heterogeneity and its functional consequences is essential for overcoming therapeutic failure.

Besides the heterogeneous molecular features of neoplastic B cells, the diversity of the tumor microenvironment (TME) also impacts the biological behavior and clinical outcomes of DLBCL patients. This heterogeneity arises not only from the TME composition, but also from the intricate intercellular

CONTACT Zhaobin Chu chuzhaobin7@163.com College of Life Sciences, University of Chinese Academy of Sciences, Beijing, 100049, China; Huilai Zhang zhanghuilai@tjmuch.com Department of Lymphoma, Tianjin Medical University Cancer Institute & Hospital, National Clinical Research Center for Cancer, Tianjin's Clinical Research Center for Cancer, Key Laboratory of Cancer Prevention and Therapy, Tianjin, 300060, China
[1] These authors contributed equally to this work.

Supplemental data for this article can be accessed online at https://doi.org/10.1080/15384047.2026.2684140.

communication within and across distinct cellular compartments.[6] Several studies have explored the prognostic significance of the TME in DLBCL, but have yielded inconsistent results. For example, some studies have linked high infiltration of FOXP3$^+$ regulatory T cells (Tregs) with improved prognosis,[7] while others have suggested an association with inferior survival. Riihijarvi et al. have observed that CD68$^+$ tumor-associated macrophages (TAMs) predicted poor outcomes in CHOP-treated patients, yet a favorable prognosis in those treated with R-CHOP.[8] Moreover, two distinct stromal gene expression signatures, stromal-1 and stromal-2, have been proposed; the stromal-1 subtype, enriched in myeloid lineage components, was associated with better survival.[9] More recently, 12 patterns of TME archetypes have been described based on single-cell data, offering partial prediction of therapeutic response.[10] However, while foundational, these studies often rely on bulk analysis or marker-based quantification, which can obscure the contributions of rare but functionally potent cell subsets and the intricate spatial crosstalk that shapes these ecosystems. Consequently, the mechanistic basis by which specific neoplastic cell states orchestrate diverse TME patterns remains largely unresolved.

Single-cell and single-nucleus RNA sequencing (sc/snRNA-seq) have emerged as powerful tools for resolving transcriptional heterogeneity and dissecting the cellular architecture of tumors at single-cell resolution. These methods enable precise delineation of malignant cell states, TME components, and their functional interactions[11]. Additionally, SpaTial Enhanced REsolution Omics-sequencing (Stereo-seq) provides nanoscale spatial transcriptomic profiling, offering insights into the spatial organization and cellular neighborhoods of both tumor and stromal cells within intact tissues.[12] To address the unmet need for high-resolution delineation of DLBCL heterogeneity, we combined snRNA-seq and Stereo-seq to construct a comprehensive single-cell atlas of DLBCL. By integrating an external scRNA-seq dataset for cross-validation,[10] we systematically characterized the malignant and immune compartments of the tumor and uncovered a previously unrecognized subset of CD3$^+$ B cells. We further elucidated the molecular programs and regulatory networks underlying this population and explored its immunosuppressive interactions with the TME. Collectively, this study provides novel insights into the cellular and spatial complexity of DLBCL, identifies a new marker of disease progression, and suggests potential therapeutic targets.

Materials and methods

This study employed an integrative multi-omics and multi-platform approach to investigate the cellular heterogeneity and tumor microenvironment of diffuse large B-cell lymphoma (DLBCL). Our experimental design encompassed four patient cohorts allocated for distinct analyzes. We performed single-nucleus RNA sequencing (snRNA-seq) on 12 fresh tumor samples and spatial transcriptomics (Stereo-seq) on two samples to generate a high-resolution transcriptomic atlas (**Table S1**). A large validation cohort of 132 formalin-fixed, paraffin-embedded (FFPE) tissues was used for immunofluorescence (IF) and immunohistochemistry (IHC) to assess clinical correlations. Furthermore, *in vitro* functional assays, including flow cytometry, transwell migration, and ELIZA, were conducted using fresh tissues from an additional 6 patients to validate cellular interactions. All studies were conducted with approval from the institutional ethics committee, and written informed consent was obtained from all participants.

For the snRNA-seq data (12 samples from this study), alignment and gene quantification were performed using Cell Ranger ARC (v2.0.0) against the GRCh38 reference genome (refdata-cellranger-arc-GRCh38-2020-A-2.0.0). Ambient RNA contamination was corrected using SoupX (v1.6.2) under default settings, in which background RNA was estimated from empty droplets and subtracted from each cell. Doublets were identified and removed using DoubletFinder (v2.0.4). pN (proportion of artificial doublets) was set to 0.25, pK (neighborhood size parameter for pANN estimation) was selected based on the BCmetric, and nExp (expected number of doublets) was estimated from a 7.5% expected doublet rate and adjusted using modelHomotypic to account for homotypic doublets. The parameter sct was set to TRUE based on SCTransform-normalized PCA space. Cells were retained if they contained at least 500 detected genes and had mitochondrial gene content ≤10%, implemented in Seurat (v4.3.0). For the scRNA-seq dataset (GSE182434, 4 samples), processed data provided by the original study were used,[10] and consistent quality control applied the same thresholds (nGene ≥ 500 and mitochondrial gene content ≤10%). For the Stereo-seq data (2 samples from this study), alignment and spatial mapping were performed using the SAW pipeline (v5.0) against the GRCh38 reference genome, generating gene

expression matrices containing spatial coordinates at the DNA nanoball (DNB) level. Cell segmentation was conducted using STOmics Cloud by aligning DNB images to nuclear staining images, followed by semi-automated segmentation based on nuclear signals to obtain cellBin-level expression matrices. CellBins were retained if featureRNA counts ranged from 200 to 8,000. Downstream analyzes, including normalization, dimensionality reduction, and clustering, were performed using Seurat (v5.0.1); 5,000 highly variable genes were selected using the vst method, 50 principal components were used, and clustering resolution was set to 0.6. Further details are provided in the **Supplementary Methods**. The overall workflow is summarized in Figure 1A.

Results

Identification and validation of CD3⁺ B cells in DLBCL

Prior to downstream analyzes, rigorous quality control was performed on the snRNA-seq data, including assessment of total UMI counts, detected gene numbers (median detected genes: 1,790), mitochondrial transcript percentages, and doublet scores (**Fig. S1A–F**). To map the cellular landscape of DLBCL, we integrated our snRNA-seq data from 12 patients with a public scRNA-seq dataset (GSE182434), yielding 137,292 cells for analysis (Figure 1A–E, **Table S2**). Unsupervised clustering identified eight major cell types, including neoplastic B cells, T cells, and myeloid populations, supported by canonical marker expression and spatial transcriptomics (Figure 1F–G, **Fig. S1G-J**).

To dissect tumor heterogeneity, we applied non-negative matrix factorization (NMF) to 64,113 neoplastic B cells, identifying four gene modules (Figure 1H, **Table S3**). Notably, Module 4 showed a T cell-like signature, with high weights for *CD3D*, *CD3E*, and *CD3G*. Scoring revealed a previously unrecognized subpopulation of neoplastic B cells co-expressing B-cell markers (*CD19*, *MS4A1*) and the CD3 complex, defined as CD3⁺ B cells (Figure 1I).

This subset was further validated across platforms. CD3⁺ B cells were detected in spatial transcriptomic data (Figure 2A). Crucially, these cells exhibited low pANN scores comparable to conventional B cells **(Fig. S1D–F)**, excluding the possibility of technical doublets. They were further validated in the external scRNA-seq cohort **(Fig. S2A)**, and showed copy number variation (CNV) patterns consistent with malignant B cells (Figure 2B**, Fig. S2B)**. Furthermore, immunofluorescence demonstrated CD3 and CD20 co-localization, and flow cytometry confirmed a CD3⁺CD20⁺ population in tumor tissues but not in peripheral blood (95% CI of difference: −5.415 to −1.293, $p = 0.0063$; Figure 2C–D**, Fig. S2C**). CD3⁺ B cells comprised ~2% of neoplastic B cells across the snRNA-seq (2.18%), scRNA-seq (2.36%), and Stereo-seq (1.51%) cohorts (Figure 2E). These findings support CD3⁺ B cells as a distinct and reproducible subpopulation in DLBCL.

CD3⁺ B cells display T cell-like transcriptomic signatures and secrete immunosuppressive TGF-β family cytokines

Transcriptomic characterization of CD3⁺ B cells revealed 4,494 upregulated genes (adjusted $p < 0.05$, $\log_2FC > 0.25$), including T-cell regulators (*CD28*, *BCL11B*) and members of the immunosuppressive TGF-β superfamily (*GDF11*, *BMP6*) (Figure 2F, **Table S4**). Consistently, functional enrichment analysis highlighted pathways related to T-cell signaling and TGF-β signaling (Figure 2G, **Table S5**). Moreover, CD3⁺ B cells displayed higher scores for T-cell exhaustion and Treg-associated gene signatures compared to cytotoxic signatures ($p < 0.0001$; **Fig. S3A-F**). Functionally, ELIZA showed that lymphocyte suspensions from tumors with higher proportions of CD3⁺ B cells secreted more BMP-6 (95% CI: 19.54 to 77.80, $p = 0.0478$) and GDF-11 (95% CI: 60.65 to 122.3, $p = 0.0476$), and less TNF-α (95% CI: -24.37 to -0.9601, $p = 0.0398$) (**Fig. S3G-K**). These data indicate that CD3⁺ B cells exhibit T cell-like features and are associated with an immunosuppressive cytokine profile.

High CD3⁺ B cell infiltration predicts poor survival in DLBCL

To evaluate the clinical relevance of CD3⁺ B cells, we quantified their abundance in 132 DLBCL patient tissues using immunofluorescence (Figure 3A,B, **Fig. S4A-I**). Patients were stratified into CD3⁺ B cell–high or low groups based on median density or count.

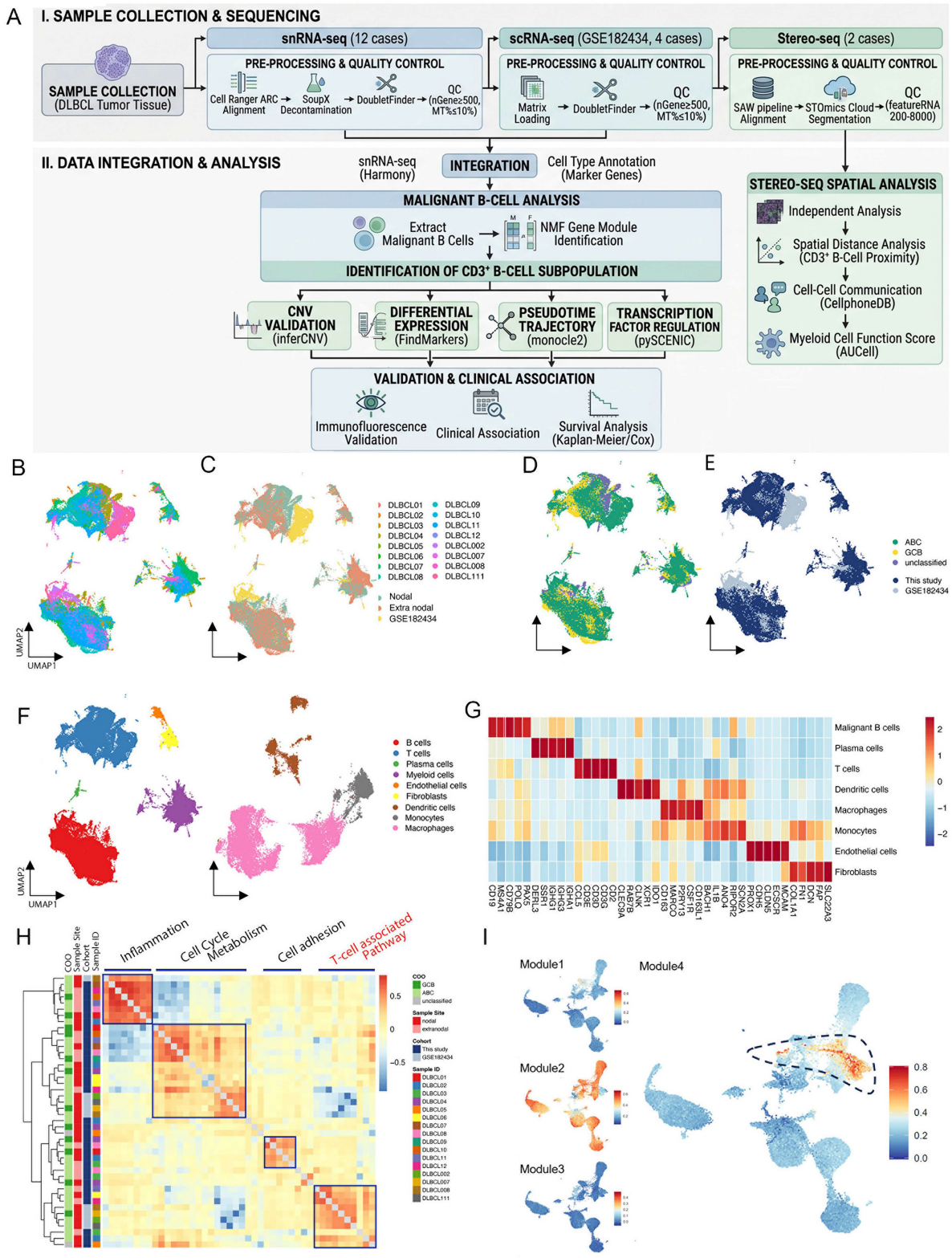

Figure 1. Single-nucleus and single-cell transcriptomic profiling of DLBCL. (A) Schematic overview of the study design and analytical workflow, including sample collection, sequencing platforms (snRNA-seq, scRNA-seq, and Stereo-seq), preprocessing and quality control steps, data integration, identification of CD3⁺ B cell subpopulation, and downstream analyzes such as CNV inference, differential expression, trajectory analysis, transcription factor regulation, and spatial transcriptomic analysis. (B–E) UMAP visualization of integrated transcriptomic data colored by sample IDs (B), sample site: nodal vs. extranodal (C), cell-of-origin (COO) subtype: germinal center B-cell–like (GCB), activated B-cell–like (ABC), and unclassified (D), and data source: this study vs. GSE182434 (E). (F) UMAP plot showing major cell types (left) and myeloid

(*Caption on next page*)

subtypes (right) identified in the integrated dataset. (G) Heatmap displaying average expression of canonical marker genes in identified cell types. (H) Heatmap of Pearson correlation coefficients between non-negative matrix factorization (NMF)-derived gene expression programs from neoplastic B cells, with annotations for sample ID, study cohort, site, and COO subtype. Four major gene modules were defined. ***(I)*** Module scores for feature genes of each module projected onto the UMAP of neoplastic B cells. The dashed line indicates the region enriched for cells with high Module 4 scores.

Kaplan–Meier analysis showed that patients with high $CD3^+$ B cell density or count had significantly shorter overall survival (OS) and progression-free survival (PFS) compared to the low group (OS: HR = 1.960, 95% CI: 1.062 to 3.620, $p = 0.0334$ for density; HR = 2.398, 95% CI: 1.299 to 4.427, $p = 0.0068$ for count; PFS: HR = 2.216, 95% CI: 1.327 to 3.701, $p = 0.0024$ for density; HR = 2.513, 95% CI: 1.543 to 4.096, $p = 0.0003$ for count; Figure 3C–D). In addition, $CD3^+$ B cell count was associated with clinical stage ($p = 0.0341$) and treatment response ($p = 0.0366$) based on Fisher's exact test (Figure 3E–F). Pairwise comparisons showed nominal differences (stage I vs. III, $p = 0.011$; complete response (CR) vs. progressive disease (PD), $p = 0.014$), which were not significant after Holm correction (adjusted $p = 0.065$ and 0.087). Trend analysis revealed a monotonic increase in $CD3^+$ B cell count with advancing stage ($p\_trend = 0.0379$) and worsening response categories ($p\_trend = 0.0205$). Logistic regression further confirmed associations with stage (OR = 1.40, 95% CI: 1.02 to 1.95, $p = 0.0398$) and response (OR = 1.46, 95% CI: 1.06 to 2.03, $p = 0.0223$), indicating that higher $CD3^+$ B cell counts are more likely to be observed in advanced disease and poorer treatment outcomes.

Multivariate Cox regression analysis was performed to identify independent prognostic factors for DLBCL. High $CD3^+$ B cell number and extranodal sites ≥2 were independently associated with both shorter PFS (HR = 2.918, 95% CI: 1.480 to 5.754, $p = 0.002$; HR = 1.808, 95% CI: 1.016 to 3.216, $p = 0.044$, respectively) and OS (HR = 2.280, 95% CI: 1.138 to 4.566, $p = 0.020$; HR = 2.831, 95% CI: 1.455 to 5.508, $p = 0.002$, respectively). Additionally, the ABC subtype and advanced stage were associated with shorter PFS (HR = 2.048, $p = 0.015$; HR = 2.946, $p = 0.006$), while bulky mass ≥ 7 cm was linked to poor OS (HR = 1.977, 95% CI: 0.999 to 3.913, $p = 0.050$) (Tables 1–2). These results indicate that high $CD3^+$ B cell infiltration is associated with adverse clinical outcomes and independently predicts poor survival in DLBCL.

CD3⁺ B cells are spatially associated with an M2-like myeloid niche

To understand how $CD3^+$ B cells shape the TME, we used spatial transcriptomics and found an enrichment of myeloid cells in close proximity (<40 μm) to $CD3^+$ B cells (Figure 4A–B). Consistently, $CD3^+$ B cells displayed more predicted interactions with myeloid subsets compared to conventional B cells (Figure 4C–D). These interactions involved TGF-β superfamily members (*BMP6*, *GDF11*) and PPAR pathways, which are associated with M2 macrophage polarization (Figure 4). In situ analysis showed that $CD163^+$ macrophages preferentially localized near $CD3^+$ B cells (Figure 4G). Moreover, myeloid cells proximal to $CD3^+$ B cells showed enriched gene signatures for angiogenesis, chemotaxis, and TGF-β signaling, suggesting that $CD3^+$ B cells are associated with an M2-like immunosuppressive niche (Figure 4H).

We functionally validated these findings in situ and in vitro. Immunofluorescence and IHC revealed greater $CD163^+$ macrophage accumulation in tumors with high $CD3^+$ B-cell infiltration ($Rs_{CD3B\ number} = 0.564$, $p < 0.001$; $Rs_{CD3B\ density} = 0.411$, $p < 0.001$; Figure 5A**, Fig. S5A-C**). While co-culture experiments showed a non-significant trend towards increased macrophage recruitment (95% CI: -4.532 to 20.60, $p = 0.1506$), supernatants from $CD3^+$ B cell–high tumors increased the proportion of $CD163^+$ macrophages (95% CI: 0.067 to 31.35, $p = 0.0494$) (Figure 5B-C). Collectively, these findings support an association between $CD3^+$ B cells and an M2-like myeloid niche.

A core transcriptional network mediates CD3⁺ B-cell reprogramming

To characterize the transcriptional programs underlying the $CD3^+$ B-cell state, we performed pseudotime analysis on malignant B cells from five snRNA-seq samples. This revealed a trajectory from conventional $CD3^-$ B cells through a transitional state to $CD3^+$ B cells (Figure 6A–C, **Fig. S6A-D**). Genes with dynamic

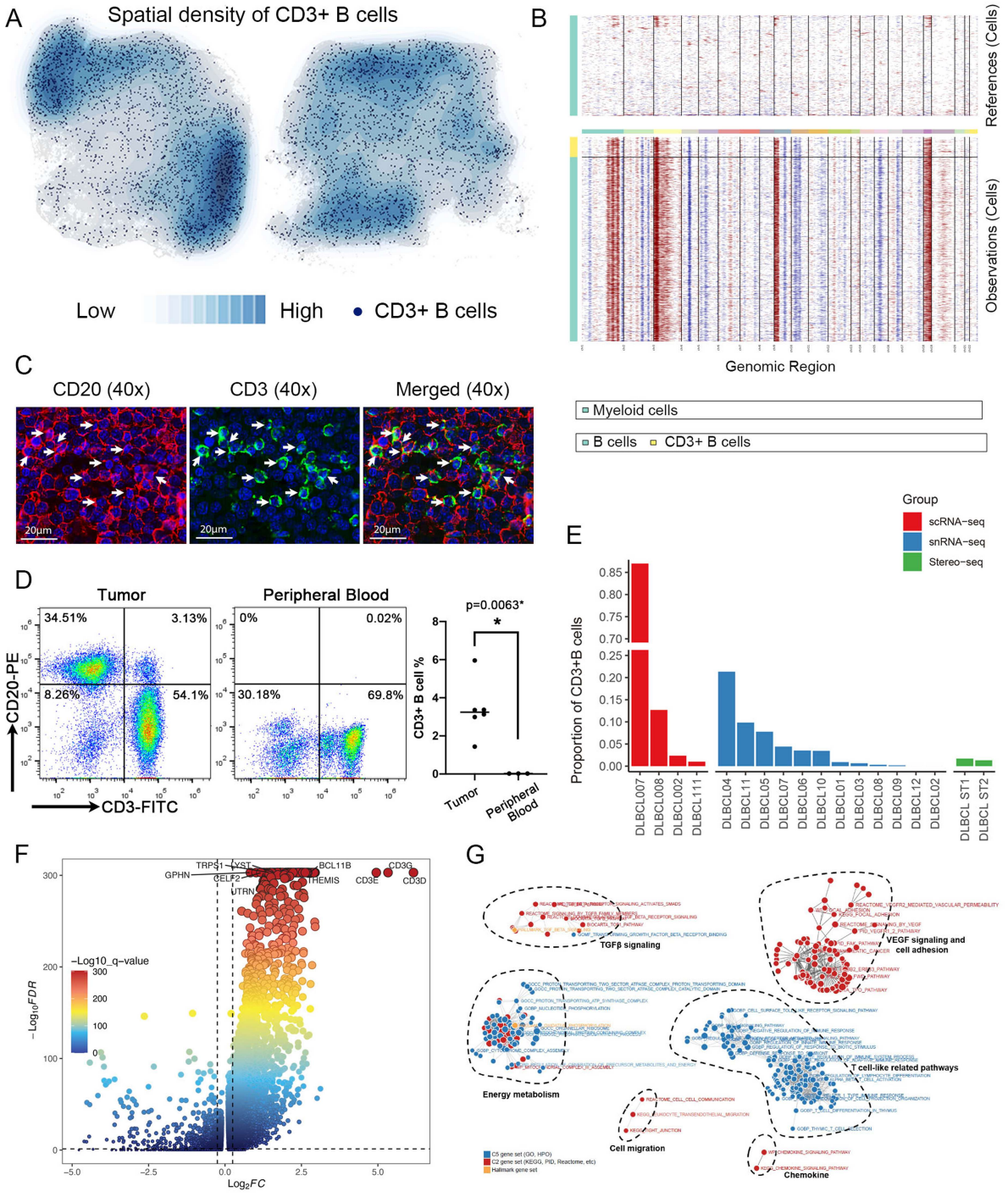

Figure 2. Validation and characterization of CD3$^+$ B cells in DLBCL. (A) Spatial distribution and density of CD3$^+$ B cells shown on Stereo-seq spatial transcriptomic maps from two DLBCL tissue sections. Blue dots represent individual CD3$^+$ B cells; the gradient bar indicates local cell density. (B) Inferred large-scale chromosomal copy number variations (CNVs) in DLBCL11 using inferCNV, with myeloid cells as reference. Gains are shown in red and losses in blue across the genome. (C) Immunofluorescence staining of DLBCL tissue. CD20 (red), CD3 (green), and nuclei (DAPI, blue). CD3$^+$ B cells are indicated by arrows. Scale bar: 20 μm. (D) Flow cytometry analysis of CD3 and CD20 expression in lymphocytes from DLBCL tissue samples ($n = 6$, including three nodal and three extranodal) and matched peripheral blood samples ($n = 3$). Summary plot shows CD3$^+$CD20$^+$ cell proportions (mean ± SEM; $p = 0.0063$, Student's t-test). (E) Proportion of CD3$^+$ B cells in all samples from snRNA-seq, scRNA-seq (GSE182434), and Stereo-seq datasets. **(F)** Volcano plot showing differentially expressed genes in CD3$^+$ B cells versus other neoplastic B cells (adjusted $p < 0.05$). (G) Network representation of gene set enrichment analysis for upregulated genes in CD3$^+$ B cells. Each node represents a significantly enriched gene set; edge width indicates similarity (Jaccard index > 0.2); colors correspond to gene set source categories.

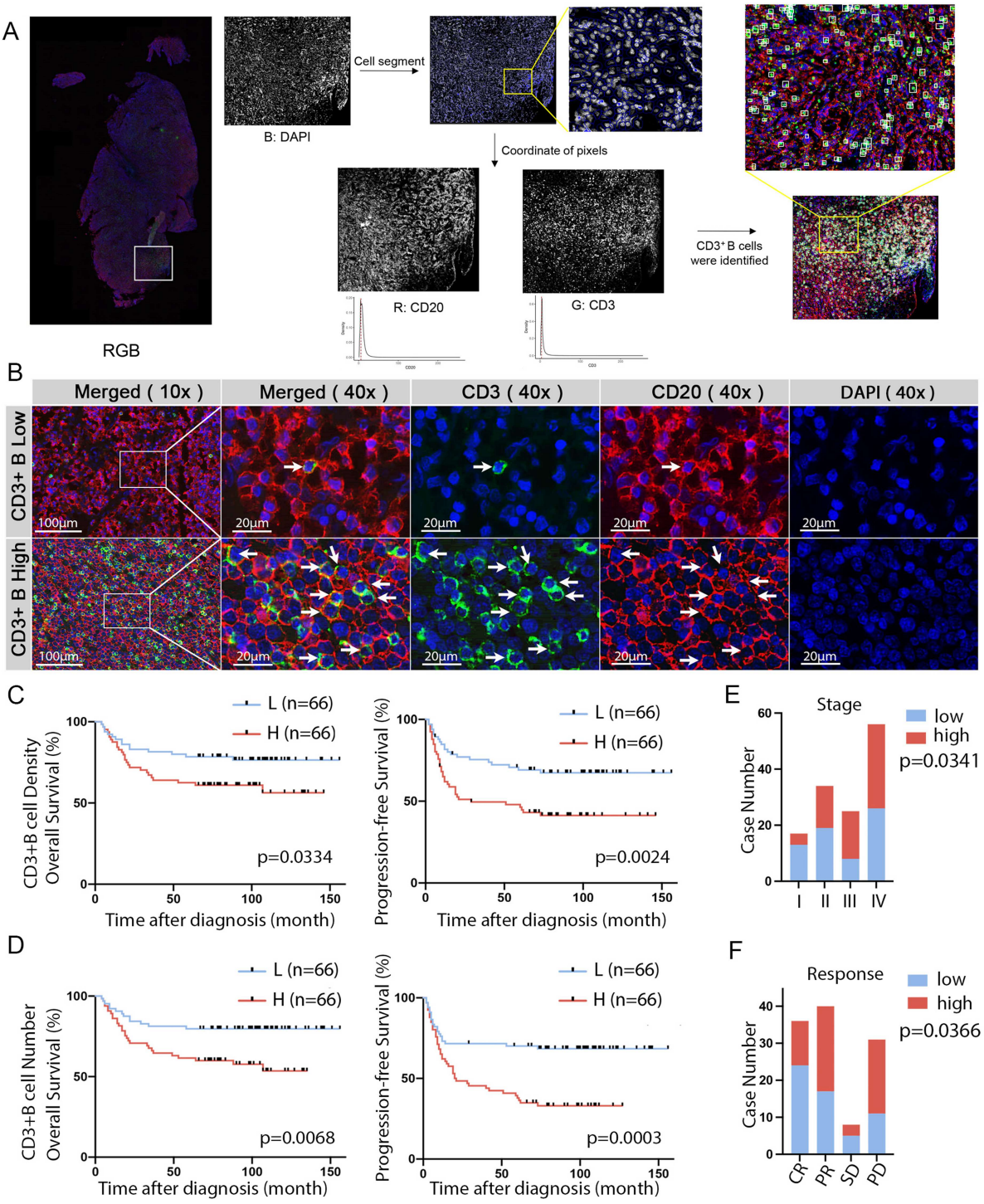

Figure 3. Immunofluorescence detection and clinical associations of CD3⁺ B cells in DLBCL. (A) Workflow for quantifying CD3⁺ B cell density using cell segmentation and fluorescence intensity of CD3 and CD20. (B) Representative images of CD20 (red), CD3 (green), and DAPI (blue) in DLBCL tissues ($n = 132$ independent patient samples). Scale bar: 20 or 100 μm. (C) Kaplan-Meier curves of overall survival (OS) and progression-free survival (PFS) stratified by CD3⁺ B cell density (high vs. low based on median). (D) Kaplan–Meier curves of OS and PFS stratified by CD3⁺ B cell number per high-power field (HPF). Threshold for high: >10 $CD20^{+}CD3^{+}$ cells/HPF. (E, F) Distribution of clinical stages (I–IV) (E) and treatment responses (CR = complete response, PR = partial response, SD = stable disease, PD = progressive disease) (F) stratified by CD3⁺ B cell number (high vs. low based on median; $n = 132$). Statistical significance was assessed using Fisher's exact test, followed by Holm correction for pairwise comparisons.

Table 1. Multivariate analysis of progression-free survival in 132 DLBCL patients.

	Univariate Analysis			Multivariate Analysis		
Cox Regression Model	HR	95%CI	*p*	HR	95%CI	*p*
Age ≥60years	1.308	0.785–2.180	0.303			
Male	1.406	0.841–2.351	0.194			
Hypertension	1.404	0.729–2.705	0.31			
Diabetes Mellitus	1.033	0.444–2.404	0.939			
ABC vs. GCB subtype	2.072	1.182–3.364	0.011*	2.048	1.152–3.642	0.015*
Advanced Stage	4.408	2.226–8.729	<0.001*	2.946	1.355–6.403	0.006*
B Symptoms	1.505	0.837–2.706	0.172			
Bulky Mass ≥7cm	1.307	0.701–2.435	0.4			
Extranodal Sites ≥2	2.201	1.319–3.675	0.003*	1.808	1.016–3.216	0.044*
Elevated LDH	1.392	0.834–2.324	0.206			
HBV Infection	1.268	0.688–2.335	0.447			
High CD3+ B cell Number	3.393	1.905–6.042	<0.001*	2.918	1.480–5.754	0.002*
High CD3+ B cell Density	1.731	1.025–2.922	0.040*	0.945	0.511–1.745	0.856

HR: Hazard Ratio; CI: Confidence Interval; ABC: Activated B-Cell; GCB: Germinal Center B-Cell; LDH: Lactate Dehydrogenase; HBV: Hepatitis B Virus.

Table 2. Multivariate analysis of overall survival in 132 DLBCL patients.

	Univariate Analysis			Multivariate Analysis		
Cox Regression Model	HR	95%CI	*p*	HR	95%CI	*p*
Age ≥ 60years	1.795	0.964–3.344	0.065			
Male	1.843	0.976–3.483	0.06			
Hypertension	1.309	0.604–2.834	0.495			
Diabetes Mellitus	1.105	0.433–2.816	0.835			
ABC vs. GCB subtype	1.272	0.672–2.409	0.46			
Advanced Stage	7.116	2.533–19.991	<0.001*	1.262	0.655–2.435	0.478
B Symptoms	1.615	0.809–3.226	0.174			
Bulky Mass ≥ 7cm	2.119	1.087–4.128	0.027*	1.977	0.999–3.913	0.050*
Extranodal Sites ≥2	2.813	1.509–5.245	0.001*	2.831	1.455–5.508	0.002*
Elevated LDH	1.599	0.866–2.952	0.134			
HBV Infection	1.022	0.503–2.078	0.952			
High CD3+ B cell Number	2.405	1.245–4.648	0.009*	2.28	1.138–4.566	0.020*
High CD3+ B cell Density	1.001	0.543–1.847	0.997			

HR: Hazard Ratio; CI: Confidence Interval; ABC: Activated B-Cell; GCB: Germinal Center B-Cell; LDH: Lactate Dehydrogenase; HBV: Hepatitis B Virus.

expression along this trajectory were grouped into three distinct clusters corresponding to early, transitional, and late states **(Table S6)**. Notably, expression of lineage-defining transcription factors (TFs), including *BCL11B*, *RUNX2*, and *RUNX3*, progressively increased along this trajectory (Figure 6D).

To identify the master regulators of this process, an integrative analysis of Regulon Specificity Scores (RSS) and Master Regulators (MR) prioritized five core TFs: *BCLAF1*, *CHURC1*, *FLI1*, *NFATC2*, and *ELF2* (Figure 6E, **Fig. S7A-B**). The activity of these TFs was positively correlated with cell adhesion ($R = 0.79$, $p < 1 \times 10^{-4}$), immune regulation ($R = 0.8$, $p < 1 \times 10^{-4}$), and TGF-β signaling ($R = 0.7$, $p < 1 \times 10^{-4}$; Figure 6F, **Fig. S8**). Network analysis further suggested that these TFs form a positive feedback circuit that activates downstream effectors, such as *NR2C2* and *IRF1*, to ultimately drive *CD3D* expression (Figure 6G**, Table S7**). Corespondingly, majority of these TFs were highly expressed in sample DLBCL04 and DLBCL007 with higher $CD3^+$ B cell abundance (**Fig. S9A-B**). Motif-based inference supported this network (Figure 6H**, Table S8**), identifying target genes that significantly overlapped with the initial Module 4 signature and correlated with its activity ($R = 0.35$, $p < 2.2 \times 10^{-16}$; **Fig. S9C-D**). Together, these data suggest that a coordinated transcriptional program underlies the $CD3^+$ B-cell state.

Validation and specificity of the $CD3^+$ B-cell transcriptional network

We validated this regulatory network through multiple approaches. First, immunofluorescence confirmed the protein expression of two core TFs, BCLAF1 and FLI1, within $CD3^+$ B cells in patient tissues (Figure 7A). Second, to support a direct regulatory role, we analyzed public ChIP-seq datasets and found a substantial overlap between our predicted targets and the promoter-bound genes of both *BCLAF1* (15.9%) and *FLI1* (8.3%) (hypergeometric test, $p < 0.05$) (Figure 7B–C, **Fig. S10A-F**).

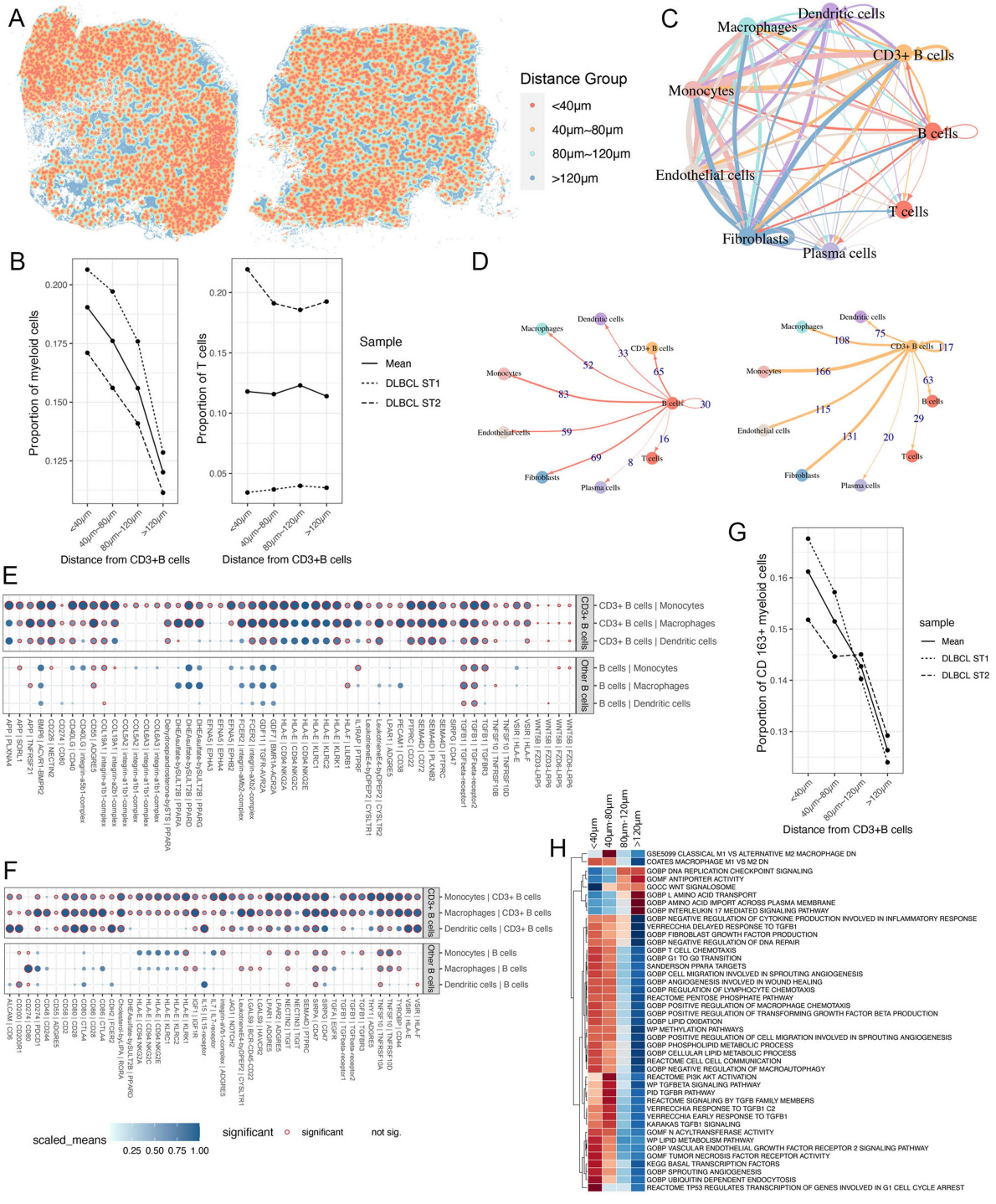

Figure 4. Spatial organization and intercellular communication associated with CD3⁺ B cells in the tumor microenvironment. (A) Spatial maps from Stereo-seq data showing individual cells stratified by proximity to the nearest $CD3^+$ B cell. Cells are color-coded into four distance intervals: < 40 μm (red), 40–80 μm (orange), 80–120 μm (light blue), and >120 μm (dark blue). (B) Distribution of myeloid cells and T cells plotted by distance from $CD3^+$ B cells across samples. Dots represent measured values at each distance interval; lines connect values across intervals for each sample and the mean. (C) Cell–cell communication network among major cell types inferred using CellphoneDB. Edges represent significant ligand–receptor interactions (FDR < 0.05). Edge thickness represents the strength of ligand-receptor interactions. (D) Comparison of ligand–receptor interaction networks between $CD3^+$ B cells (right) and conventional B cells (left) with other cell populations. (E) Dot plot illustrating ligand-receptor interactions between $CD3^+$ or conventional B cells to myeloid cells. Ligands are expressed on B cells and receptors on myeloid cells. (F) Dot plot illustrating ligand-receptor interactions from myeloid cells to $CD3^+$ or conventional B cells. Ligands are expressed on myeloid cells and receptors on B cells. Dot size indicates the proportion of cells expressing the ligand–receptor pair. Color represents scaled mean

(*Caption on next page*)

expression. Significant interactions are defined as FDR < 0.05. (G) Distribution of CD163$^+$ myeloid cells plotted by distance from CD3$^+$ B cells. (H) Heatmap showing averaged gene set scores representing pathway activities in myeloid cells stratified by distance from CD3$^+$ B cells. Scores were calculated using AUCell. Rows represent gene sets (MSigDB). Columns represent distance-defined cell groups.

Furthermore, all five core TFs exhibited significantly higher activity in CD3$^+$ B cells compared to both conventional neoplastic and normal B cells ($p < 0.0001$), underscoring their specific role in establishing this aberrant transcriptional state (Figure 7D). This TF network likely orchestrates the CD3$^+$ phenotype, linking it to an immunosuppressive TME (Figure 7E) and a functional state of increased self-renewal, as evidenced by the enrichment of proliferative and cancer stem cell gene signatures in CD3$^+$ B cells ($p < 0.0001$; **Fig. S11A-C**). These results support this network as a defining feature of CD3$^+$ B cells.

Discussion

In this study, we identified and characterized a previously unrecognized subset of neoplastic B cells in DLBCL that aberrantly express the T-cell antigen CD3. Our high-resolution analyzes revealed that this CD3$^+$ B-cell subset is a recurrent, albeit low-abundance, feature across multiple patients, distinguishing it from rare case reports of diffuse CD3 positivity.[13-23] We demonstrate that this population is defined by a core transcriptional regulatory network, is spatially associated with M2-like macrophages, and is related to an immunosuppressive niche. Clinically, a higher abundance of these CD3$^+$ B cells independently predicted advanced disease and inferior overall survival, establishing a direct link between this unique cell state and adverse clinical outcomes.

Aberrant expression of T cell-associated antigens in B-cell neoplasms has been previously reported. For example, Inaba et al. have identified co-expression of at least one T cell antigen in 24.2% of B-cell lymphoma cases by flow cytometry,[24] and Tsuyama et al. have reported similar expression patterns in 25% of DLBCL and other mature B-cell lymphoma cases by IHC.[25] However, specific CD3 expression in neoplastic B cells of DLBCL has only been documented in approximately 30 case studies.[13,15,19,20,22,23] These rare cases were characterized by diffuse and uniform staining of CD3 across tumor sections, representing a highly unusual phenotype in which most tumor cells exhibit T-cell-like features. In contrast, the CD3$^+$ B cell subset identified in our study comprised a median of only 2.14% of neoplastic B cells, but was consistently present in most patient samples. This finding was validated by IF and flow cytometry in our cohort and further supported by analysis of an external scRNA-seq dataset (GSE182434). In that dataset, case DLBCL007 exhibited widespread CD3 expression in 86.99% of B cells, resembling previously reported rare cases, whereas other samples showed a median CD3$^+$ B cell frequency of 2.36%, closely matching our observations. These results highlight the strength of our high-resolution transcriptomic profiling in revealing a previously underappreciated but recurrent subpopulation of CD3$^+$ B cells in DLBCL.

This distinct prevalence pattern of CD3$^+$ B cells likely reflects divergent underlying causes. In previous case reports of CD3$^+$ DLBCL, the majority of patients exhibited underlying immune dysfunction, including EBV infection, HIV infection, organ transplantation, or other immunodeficiencies, coinciding with extensive and diffuse CD3 expression in the B cell population.[20,22,23] The broad, remarkably high percentage of CD3$^+$ B cells in sample DLBCL007 from GSE182434 (86.99%) may reflect a similar etiology, although clinical metadata are unavailable for confirmation. Other than this outlier, the highest CD3$^+$ B cell proportion was observed in sample DLBCL04 (21.33%), which was diagnosed as EBV-associated DLBCL, further supporting this association. In contrast, the majority of our cohort harbored a small but consistent CD3$^+$ B cell subset (median 2.14%), suggesting a unique, transcriptionally regulated mechanism. Pseudotime trajectory and gene regulatory network analyzes revealed a core transcriptional circuit comprising FLI1, BCLAF1, CHURC1, NFATC2, and ELF2, which progressively activates CD3D expression along the transition to the CD3$^+$ state. Among these, FLI1, a hematopoietic ETS family TF essential for immune cell development,[26,27] has been reported to be recurrently amplified at 11q24.3 in ~25% of DLBCL cases, driving overexpression and contributing to tumor proliferation and differentiation arrest.[28] ChIP-seq data further supported FLI1 and BCLAF1 binding to the promoter region of CD3D and other network genes, reinforcing their role in establishing this phenotype. Notably, all five TFs were highly

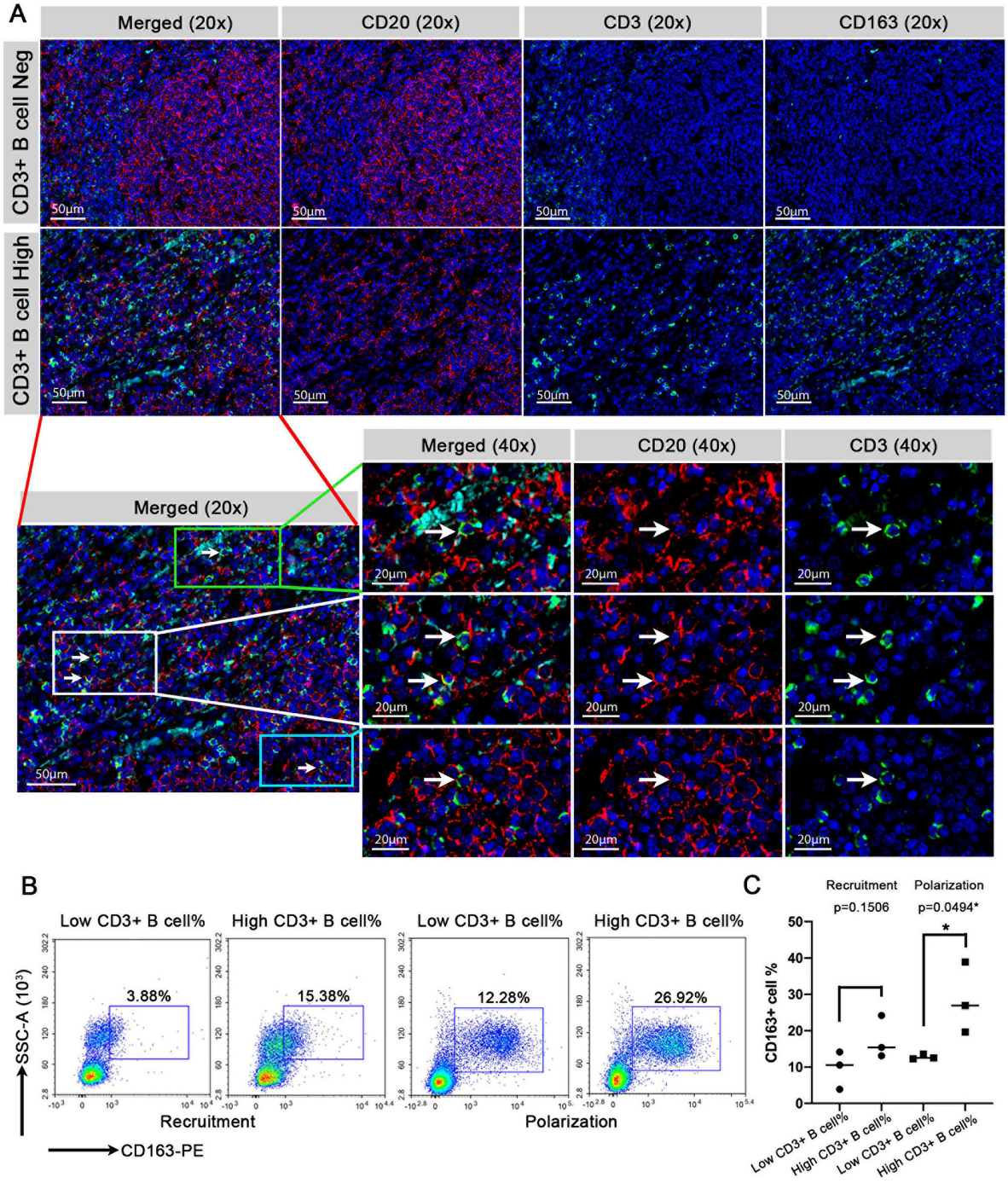

Figure 5. Validation of functional interaction between $CD3^+$B cells and macrophages. (A) Representative immunofluorescence images of DLBCL tissues with high $CD3^+$ or negative $CD3^+$ B cell infiltration ($n = 6$ biological replicates). Sections were stained for CD20 (red), CD3 (green), CD163 (light blue), and DAPI (blue). Upper panels: overview (20×); lower panels: enlarged views (40×) of boxed regions. Scale bars: 50 μm (overview) and 20 μm (magnified). White arrows indicate $CD3^+CD20^+CD163^+$ cells. (B) Flow cytometry plots showing $CD163^+$ macrophages among PBMCs following transwell recruitment (left; migration toward lymphocyte suspensions) or polarization (right; stimulation with tumor-derived supernatants) assays. PBMCs were exposed to samples derived from DLBCL tissues with high or low $CD3^+$ B cell proportions. (C) Quantification of $CD163^+$ macrophage percentages in recruitment and polarization assays. Data are presented as mean ± standard error of the mean (SEM); $n = 3$ biological replicates per group. Statistical comparisons were performed using Student's t-test.

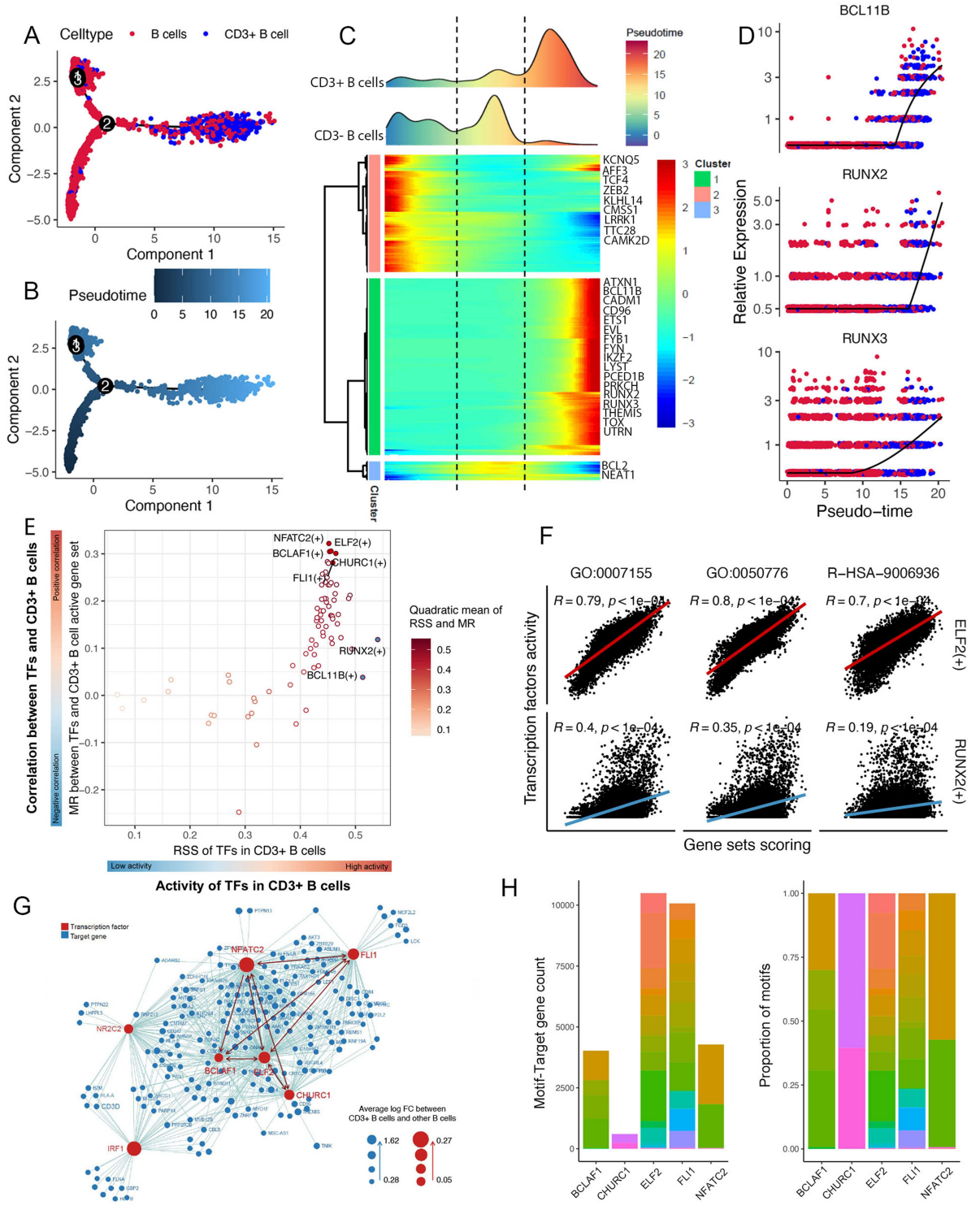

Figure 6. Transcriptional regulatory landscape of CD3⁺ B cells. (A, B) Pseudotime trajectory analysis of neoplastic B cells in sample DLBCL11, colored by cell type (A) and pseudotime (B). Cells are positioned along an inferred trajectory representing progression from CD3⁻ to CD3⁺ B cells. (C) Heatmap of gene expression dynamics along pseudotime. Genes were grouped into three clusters based on temporal expression profiles. Pink: genes enriched in CD3⁻ B cells; Green: genes enriched in CD3⁺ B cells; Blue: genes enriched in transition cells. (D) Expression patterns of representative transcription factors (TFs) (BCL11B, RUNX2, RUNX3) across the three clusters. (E) Scatter plot showing regulon specificity scores (RSS, cell-type-specific TF activity) and mean functional correlation coefficients (MR, average correlation between TF activity and gene set scores) for TFs in CD3⁺ B cells. (F) Correlation between TF activity (regulon AUC scores) and selected gene sets related to cell adhesion (GO:0007155), immune response (GO:0050776), and TGF-β signaling (R-HSA-9006936). Each point represents a gene set; lines indicate linear regression. (G) Diagram of transcriptional regulatory network involving key TFs

(*Caption on next page*)

and downstream effectors. Nodes represent TFs (red) and target genes (blue); edges indicate predicted regulatory relationships inferred by SCENIC. (H) Overview of motif-based transcriptional regulation. Left: number of target genes per transcription factor. Right: motif composition associated with each transcription factor, color-coded by motif identity.

expressed in sample DLBCL04, indicating that this regulatory program operates broadly, independent of immune dysfunction, and may represent a generalizable transcriptional route through which neoplastic B cells aberrantly acquire T cell features. These findings suggest that at least two non-mutually exclusive mechanisms may underlie CD3+ B-cell emergence in DLBCL. In cases associated with immune dysfunction or EBV infection, a broad phenotypic shift can lead to widespread CD3 expression in the malignant population, as observed in DLBCL007 and DLBCL04. In contrast, in most patients, a smaller but recurrent CD3+ B-cell subset likely arises through an intrinsic transcriptional program involving FLI1 and related regulators. This dual model integrates both extrinsic and intrinsic routes to aberrant lineage antigen expression.

Before our study, the biological significance of CD3+ B cells in DLBCL, particularly as a low-abundance neoplastic subset, was largely undetermined. While earlier studies using flow cytometry or IHC often reported diffuse CD3 expression, our integration of sc/snRNA-seq and Stereo-seq resolved this population as a unique minor subset. This allowed for clinical correlation analyzes, revealing that higher $CD3^+$ B cell proportions were associated with worse prognosis. An interesting observation from our clinical analysis was that the number of CD3+ B cells, rather than their density, emerged as an independent prognostic factor. This difference suggests that the total burden of this immunosuppressive subset, rather than its concentration within specific tissue regions, is more critical in promoting systemic disease progression. Alternatively, manual counting by pathologists may provide more accurate quantification by mitigating potential artifacts in automated fluorescence-based density measurements, such as signal saturation or background noise. Future studies employing standardized quantitative pathology approaches will be needed to determine the optimal method for evaluating this biomarker's clinical utility.

Transcriptomic profiling showed that, apart from aberrant CD3D expression, this subset was enriched in immunoregulatory and chemotactic mediators, including TGFB1, BMP6, GDF11, LGALS1, and CXCL16. Gene set enrichment analyzes indicated activation of TGF-β signaling, cytokine–cytokine receptor interaction, and PPAR pathways, all of which have been implicated in immune suppression and macrophage polarization. These features suggest that CD3+ B cells may influence the tumor immune microenvironment through secretion of immunomodulatory factors and recruitment of suppressive myeloid cells, consistent with their spatial proximity to macrophages and their inferred function in remodeling the TME. Differential expression was evaluated with a relatively modest fold-change cutoff ($Log_2FC \geq 0.25$), reflecting the subtle transcriptional differences among $CD3^+$ B cell subsets and underscoring the value of single-cell resolution in capturing such heterogeneity.

The observed CD3+ B-cell-associated microenvironment aligns with emerging models of spatially organized and genetically influenced TME heterogeneity in DLBCL. Recent multimodal spatial analyzes have demonstrated that DLBCL tumors are structured into discrete cellular niches with distinct patterns of immune cell interaction and functional states,[29] supporting our finding that CD3+ B cells are preferentially associated with localized myeloid-enriched regions. In addition, genetic studies have emphasized that lymphoma-intrinsic alterations actively shape TME composition and promote immunosuppressive states through cytokine signaling and cellular reprogramming,[30] which is consistent with the transcriptionally defined TGF-β-rich program observed in CD3+ B cells. Moreover, recent single-cell analyzes have highlighted that immune cell heterogeneity,[31] particularly within T-cell compartments, has strong prognostic relevance in DLBCL, whereas our data extend this paradigm by identifying a CD3+ B cell subset that exhibits T cell-like features and is independently associated with adverse outcomes. Taken together, these results suggest that CD3+ B cells may represent a tumor-intrinsic component associated with localized immune suppression and microenvironmental heterogeneity in DLBCL.

In previous studies of DLBCL, infiltrating myeloid cells have received less attention than T cells, and their role remains controversial. For example, the "stromal-1" signature identified by Lenz et al. was enriched in macrophages and extracellular matrix and associated with favorable prognosis.[9] Similarly, $CD68^+$ macrophages predicted improved outcome in R-CHOP-treated patients.[8] Conversely, several

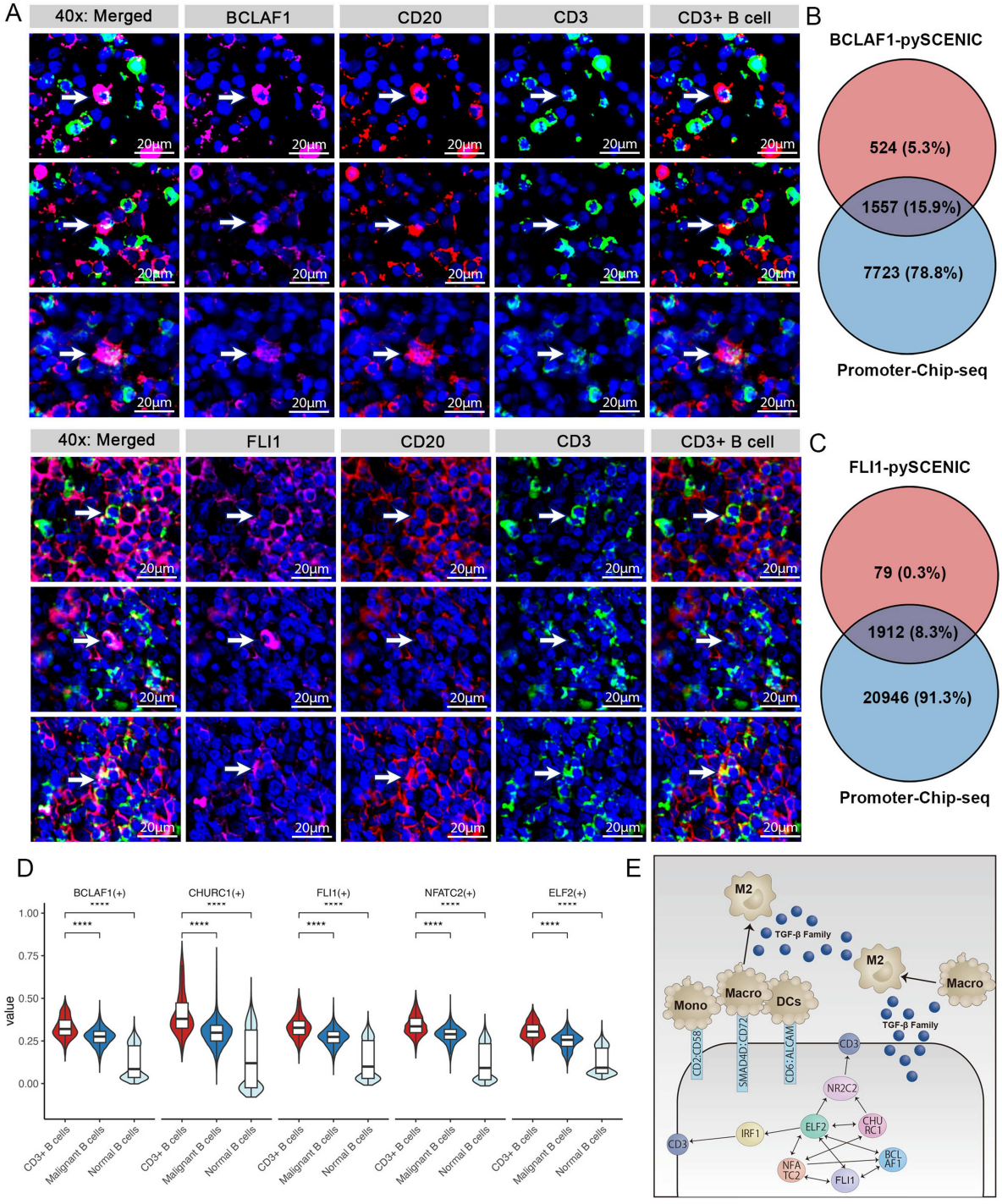

Figure 7. Validation and specificity of the transcriptional network in CD3⁺ B cells. (A) Representative immunofluorescence images showing BCLAF1 and FLI1 expression in $CD3^+$ B cells from fresh DLBCL tumor tissues ($n = 6$ biological replicates). Green: CD3; Red: CD20; Purple: BCLAF1 or FLI1; Blue: DAPI. White arrows indicate CD3⁺CD20⁺ cells co-expressing the indicated transcription factors. Magnification: 40×. Scale bar: 20 μm. (B, C) Venn diagrams showing overlap between pySCENIC-inferred target genes and promoter-bound genes from ChIP-seq datasets for BCLAF1 (B) and FLI1 (C). Overlap significance was assessed by hypergeometric test. (D) Violin plots depicting transcription factor activity (BCLAF1, CHURC1, FLI1, NFATC2, ELF2) in $CD3^+$ B cells, conventional neoplastic B cells, and normal B cells. (E) Schematic model of the regulatory network involving these TFs and their potential influence on CD3 expression and the immune microenvironment. Arrows indicate predicted regulatory or signaling relationships.

studies have demonstrated that M2-like macrophages correlated with poor prognosis.[32] Recent scRNA-seq analyzes have identified myeloid subclusters in limited DLBCL samples,[33] and spatial profiling study confirmed that macrophage signatures predict inferior survival compared to reactive lymphoid tissues.[34] Building on these findings, we explored the spatial organization and functional modulation of myeloid subsets by CD3+ B cells. Stereo-seq analysis revealed that CD3+ B cells were frequently surrounded by myeloid cells, particularly M2-like macrophages, a pattern confirmed by mIF. It should be noted that macrophage states are heterogeneous and not strictly dichotomous. Although CD163 is a widely recognized marker for M2-like, anti-inflammatory macrophages, relying on a single marker may not fully capture the complex spectrum of M2 phenotypes. A more comprehensive definition often involves the complementary evaluation of additional markers, such as CD206 (MRC1) and ARG1.[35] Communication analysis identified elevated expression of TGF-β superfamily members (e.g. BMP6, GDF11) in CD3+ B cells, which engage TGF-β receptors and activate canonical Smad signaling.[36] This axis promotes recruitment and M2 polarization of TAMs,[37-39] consistent with our enrichment analysis of CD3+ B cells and validated by transwell and polarization assays. Gene expression of macrophages adjacent to CD3+ B cells exhibited features of M2 phenotype, including angiogenesis, migration, and TGF-β signaling.[40,41] These findings suggest that CD3+ B cells are associated with the local immune microenvironment involving TGF-β-dependent macrophage modulation.

The immunosuppressive remodeling of the TME by CD3+ B cells may underlie their clinical impact. Across our cohort, patients with higher proportions of CD3+ B cells exhibited significantly worse OS, more advanced disease stage, and reduced rates of complete response following frontline treatment. This correlation was further validated in the external scRNA-seq dataset. Given their association with M2 macrophage enrichment, a cell type known to promote immune evasion, angiogenesis, and tumor dissemination, CD3+ B cells likely contribute to an immunosuppressive niche that facilitates disease progression. Thus, the CD3+ B cell subset represents both a mechanistic driver of immune remodeling and a potential prognostic indicator for DLBCL patients.

Our findings also raise translational opportunities. Pharmacologic targeting of FLI1 has been actively explored. Inhibitors such as TK-216 and mithramycin analogs are under clinical evaluation in Ewing sarcoma.[42] Diterpenoid compounds have been shown to directly block its DNA-binding activity in leukemia models.[43] In addition, TGF-β pathway inhibitors, including neutralizing antibodies, ligand traps, and receptor kinase inhibitors, have been tested in solid tumors and hematologic cancers. However, their efficacy is limited by systemic toxicity and variable effects on immune regulation.[44] Integrating such strategies into DLBCL regimens may counteract FLI1-mediated transcriptional reprogramming and TGF-β–induced macrophage polarization, thereby mitigating the immunosuppressive effects of CD3+ B cells.

This study has several limitations. First, as an exploratory, multimodal integrative analysis, a formal prospective power calculation was not performed. Sample sizes were determined based on sample availability and sequencing cost. Although we analyzed a total of 16 single-cell samples to consistently identify the CD3+ B cell subset and validated the clinical association in a cohort of 132 DLBCL patients, the sample size used for *in vitro* functional validation was limited, potentially contributing to the lack of statistical significance in some assays. In addition, spatial transcriptomic analyzes were performed on a limited number of samples, which may affect the generalizability of spatial interaction patterns. Second, the upstream events responsible for initiating the TF regulatory network remain unclear. Additional epigenetic or extrinsic factors may participate in triggering this aberrant program. Third, the study lacks in vivo validation of CD3+ B cell–macrophage interactions due to the absence of an immunocompetent DLBCL model representing this subset. Future studies incorporating lineage-tracing, genetic perturbation, and humanized mouse models will be essential to confirm these findings and evaluate therapeutic targeting strategies.

In conclusion, this study identified a distinct CD3+ B cell subset in DLBCL and revealed its transcriptional regulation, its role in creating an M2 macrophage-enriched immunosuppressive microenvironment, and its strong association with poor clinical outcomes. These findings advance our understanding of DLBCL heterogeneity and establish this subset as a promising prognostic biomarker. Key molecular regulators, including the TF *FLI1* and the TGF-β signaling axis, represent promising candidate therapeutic targets.

Acknowledgments

Mingxiao Lang designed the project and participated in all stages of the work. Zhaobin Chu performed bioinformatics analysis. Youqin Feng processed tumor tissues and constructed a library for snRNA-seq. Li Zhou completed the quality control of the data. Bin Li collected and processed tumor tissues for Stereo-seq and flow cytometry, and further performed experiments, including flow cytometry, transwell, and ELIZA. Jing Zhao performed immunofluorescence and immunohistochemistry assays. Wei Li performed survival and clinical analysis. Lanfang Li, Lihua Qiu, Zhengzi Qian, Shiyong Zhou, and Huilai Zhang provided biopsy tissues for snRNA-seq. Kexin Chen assisted in the bioinformatics analysis. Mingxiao Lang wrote the manuscript. Zhaobin Chu supervised throughout the program and revised the manuscript. All authors read and approved the final manuscript.

Author contributions

CRediT: **Mingxiao Lang:** Conceptualization, Data curation, Formal analysis, Investigation, Methodology, Writing – original draft, Writing – review & editing; **Youqin Feng:** Investigation, Methodology, Writing – review & editing; **Li Zhou:** Data curation, Validation, Writing – review & editing; **Bin Li:** Investigation, Methodology, Writing – review & editing; **Wei Li:** Formal analysis, Writing – review & editing; **Jing Zhao:** Investigation, Methodology, Writing – review & editing; **Kexin Chen:** Formal analysis, Writing – review & editing; **Lanfang Li:** Data curation, Resources, Writing – review & editing; **Lihua Qiu:** Data curation, Resources, Writing – review & editing; **Zhengzi Qian:** Data curation, Resources, Writing – review & editing; **Shiyong Zhou:** Data curation, Resources, Writing – review & editing; **Huilai Zhang:** Data curation, Resources, Writing – review & editing; **Zhaobin Chu:** Formal analysis, Supervision, Writing – review & editing.

Disclosure statement

The authors declare that they have no competing interests.

Funding

This work was supported by the National Natural Science Foundation of China (81702427), the Joint Funds of the Natural Science Foundation of Tianjin (No. 25JCLMJC00430), the Tianjin Medical University Cancer Hospital and Institute Cultivation Program (230203), and the Tianjin Key Medical Discipline (Specialty) Construction Project (TJYXZDXK-009A).

ORCID

Zhaobin Chu 0009-0006-8764-7916

Data availability statement

The data that support the findings of this study are openly available in the CNGB Sequence Archive (CNSA) of the China National GeneBank DataBase (CNGBdb) at https://db.cngb.org/, reference number CNP0005628.[45,46] Supplementary Table 3-8 are available in figshare at https://doi.org/10.6084/m9.figshare.31180999. Other data were derived from the following resources available in the public domain: Gene Expression Omnibus (GEO) at https://www.ncbi.nlm.nih.gov/geo/, reference number GSE182434, GSE32465, GSE157191.

Ethics approval statement

The study was approved by the ethics committee of Tianjin Medical University Cancer Institute and Hospital (No. bc2022089). All participants were informed about the study protocol and provided written informed consent to participate in the study. I confirm that all methods were performed in accordance with the relevant guidelines. All procedures were performed in accordance with the ethical standards laid down in the 1964 Declaration of Helsinki and its later amendments.

References

1. Sehn LH, Salles G. Diffuse large B-Cell lymphoma. NEJM. 2021;384(9):842–858. doi: 10.1056/NEJMra2027612.
2. Roschewski M, Staudt LM, Wilson WH. Diffuse large B-cell lymphoma-treatment approaches in the molecular era. Nat Rev Clin Oncol. 2014;11(1):12–23. doi: 10.1038/nrclinonc.2013.197.

3. Pasqualucci L, Dalla-Favera R. Genetics of diffuse large B-cell lymphoma. Blood. 2018;131(21):2307–2319. doi: 10.1182/blood-2017-11-764332.
4. Schmitz R, Wright GW, Huang DW, Johnson CA, Phelan JD, Wang JQ, Roulland S, Kasbekar M, Young RM, Shaffer AL, et al. Genetics and pathogenesis of diffuse large B-Cell lymphoma. NEJM. 2018;378(15):1396–1407. doi: 10.1056/NEJMoa1801445.
5. Wright GW, Huang DW, Phelan JD, Coulibaly ZA, Roulland S, Young RM, Wang JQ, Schmitz R, Morin RD, Tang J, et al. A probabilistic classification tool for genetic subtypes of diffuse large B cell lymphoma with therapeutic implications. Cancer Cell. 2020;37(4):551–568 e514. doi: 10.1016/j.ccell.2020.03.015
6. Vitale I, Manic G, Coussens LM, Kroemer G, Galluzzi L. Macrophages and metabolism in the tumor microenvironment. Cell Metab. 2019;30(1):36–50. doi: 10.1016/j.cmet.2019.06.001.
7. Bai Y, He T, Zhang L, Liu Q, Yang J, Zhao Z, Yang K, Zhang M. Prognostic value of FOXP3(+) regulatory T cells in patients with diffuse large B-cell lymphoma: a systematic review and meta-analysis. BMJ Open. 2022;12(9):e060659. doi: 10.1136/bmjopen-2021-060659.
8. Riihijarvi S, Fiskvik I, Taskinen M, Vajavaara H, Tikkala M, Yri O, Karjalainen-Lindsberg ML, Delabie J, Smeland E, Holte H, et al. Prognostic influence of macrophages in patients with diffuse large B-cell lymphoma: a correlative study from a nordic phase II trial. Haematologica. 2015;100(2):238–245. doi: 10.3324/haematol.2014.113472.
9. Lenz G, Wright G, Dave SS, Xiao W, Powell J, Zhao H, Xu W, Tan B, Goldschmidt N, Iqbal J, et al. Stromal gene signatures in large-B-cell lymphomas. NEJM. 2008;359(22):2313–2323. doi: 10.1056/NEJMoa0802885.
10. Steen CB, Luca BA, Esfahani MS, Azizi A, Sworder BJ, Nabet BY, Kurtz DM, Liu CL, Khameneh F, Advani RH, et al. The landscape of tumor cell states and ecosystems in diffuse large B cell lymphoma. Cancer Cell. 2021;39(10):1422–1437 e1410. doi: 10.1016/j.ccell.2021.08.011.
11. Slyper M, Porter CB, Ashenberg O, Waldman J, Drokhlyansky E, Wakiro I, Smillie C, Smith-Rosario G, Wu J, Dionne D. A single-cell and single-nucleus RNA-Seq toolbox for fresh and frozen human tumors. Nat Med. 2020;26(5):792–802. doi: 10.1038/s41591-020-0844-1.
12. Wu L, Yan J, Bai Y, Chen F, Zou X, Xu J, Huang A, Hou L, Zhong Y, Jing Z, et al. An invasive zone in human liver cancer identified by stereo-seq promotes hepatocyte-tumor cell crosstalk, local immunosuppression and tumor progression. Cell Res. 2023;33(8):585–603. doi: 10.1038/s41422-023-00831-1.
13. Baker J, Zadeh SL, Aguilera NS. ALK-positive large B-cell lymphoma (ALK + LBCL) with aberrant CD3 expression. J Hematop. 2024;17(2):109–114. doi: 10.1007/s12308-024-00582-x.
14. Nicoletti A, Aresu L, Marino M, Massaro M, Martignani E, Caporali E, Capuccini S, Bonfanti U, Gola C. CD3-CD20-positive nodal lymphoma with cross-lineage rearrangement in a dog. J Vet Diagn Invest. 2020;32(6):964–967. doi: 10.1177/1040638720963132.
15. Oliveira JL, Grogg KL, Macon WR, Dogan A, Feldman AL. Clinicopathologic features of B-Cell lineage neoplasms with aberrant expression of CD3: a study of 21 cases. Am J Surg Pathol. 2012;36(9):1364–1370. doi: 10.1097/PAS.0b013e31825e63a9.
16. Pan Z, Chen M, Zhang Q, Wang E, Yin L, Xu Y, Huang Q, Yuan Y, Zhang X, Zheng G, et al. CD3-positive plasmablastic B-cell neoplasms: a diagnostic pitfall. Mod Pathol. 2018;31(5):718–731. doi: 10.1038/modpathol.2017.177.
17. Ponzo G, Umana GE, Valastro M, Giuffrida M, Tranchina MG, Nicoletti GF, Scalia G. Cervical radiculopathy as first presentation of CD3-positive diffuse large B-cell lymphoma of the cervico-thoracic junction. Br J Neurosurg. 2023;37(5):1190–1193. doi: 10.1080/02688697.2020.1828278.
18. Wallentine JC, Perkins SL, Tripp SR, Bruggman RD, Bayerl MG. Diffuse large B-cell lymphoma with coexpression of CD3 in a pediatric patient: a case report, review of the literature, and tissue microarray study. J Pediatr Hematol Oncol. 2009;31(2):124–127. doi: 10.1097/MPH.0b013e31818b354a.
19. Wang E, Stoecker M. Primary mediastinal (thymic) large B cell lymphoma with aberrant expression of CD3: a case report with review of the literature. Int J Hematol. 2010;91(3):509–515. doi: 10.1007/s12185-010-0501-4.
20. Wang J, Chen C, Lau S, Raghavan RI, Rowsell EH, Said J, Weiss LM, Huang Q. CD3-positive large B-cell lymphoma. Am J Surg Pathol. 2009;33(4):505–512. doi: 10.1097/PAS.0b013e318185d231.
21. Wong YP, Masir N, Chew MX. CD3-positive plasmablastic lymphoma reported in two cases: a potential diagnostic caveat. Indian J Pathol Microbiol. 2021;64(3):579–583. doi: 10.4103/IJPM.IJPM_616_20.
22. Wu B, Vallangeon B, Galeotti J, Sebastian S, Rehder C, Wang E. Epstein-barr virus-negative diffuse large B cell lymphoma with aberrant expression of CD3 and other T cell-associated antigens: report of three cases with a review of the literature. Ann Hematol. 2016;95(10):1671–1683. doi: 10.1007/s00277-016-2749-0.
23. Yang LH, Ingersoll K, Zhao Y, Luedke C, Sebastian S, Wang E. CD3-positive diffuse large B-cell lymphoma relapses as CD3-negative large B-cell lymphoma: loss of aberrant antigen expression in B-cell lymphoma after chemotherapy. Pathol Res Pract. 2018;214(10):1738–1744. doi: 10.1016/j.prp.2018.07.003.
24. Inaba T, Shimazaki C, Sumikuma T, Nakagawa M. T-cell associated antigen-positive B-cell lymphoma. Leuk Lymphoma. 2001;42(6):1161–1171. doi: 10.3109/10428190109097741.
25. Tsuyama N, Ennishi D, Yokoyama M, Baba S, Asaka R, Mishima Y, Terui Y, Hatake K, Takeuchi K. Clinical and prognostic significance of aberrant T-cell marker expression in 225 cases of de novo diffuse large B-cell lymphoma and 276 cases of other B-cell lymphomas. Oncotarget. 2017;8(20):33487–33500. doi: 10.18632/oncotarget.16532.

26. Priebe V, Sartori G, Napoli S, Chung EYL, Cascione L, Kwee I, Arribas AJ, Mensah AA, Rinaldi A, Ponzoni M, et al. Role of ETS1 in the transcriptional network of diffuse large B cell lymphoma of the activated B cell-like type. Cancers (Basel). 2020;12(7):1912. doi: 10.3390/cancers12071912.
27. Zhang XK, Moussa O, LaRue A, Bradshaw S, Molano I, Spyropoulos DD, Gilkeson GS, Watson DK. The transcription factor Fli-1 modulates marginal zone and follicular B cell development in mice. J Immunol. 2008;181(3):1644–1654. doi: 10.4049/jimmunol.181.3.1644.
28. Bonetti P, Testoni M, Scandurra M, Ponzoni M, Piva R, Mensah AA, Rinaldi A, Kwee I, Tibiletti MG, Iqbal J, et al. Deregulation of ETS1 and FLI1 contributes to the pathogenesis of diffuse large B-cell lymphoma. Blood. 2013;122(13):2233–2241. doi: 10.1182/blood-2013-01-475772.
29. Dai Y, Kizhakeyil A, Chihara D, Li X, Liu Y, Sainz Zuniga TP, Wilson A, Henderson J, Vibe D, Petrosyants A. Multi-modal spatial characterization of tumor immune microenvironments identifies targetable inflammatory niches in diffuse large B cell lymphoma. Nat Genet. 2025;57:1–13.
30. Cerchietti L. Genetic mechanisms underlying tumor microenvironment composition and function in diffuse large B-cell lymphoma. Blood. 2024;143(12):1101–1111. doi: 10.1182/blood.2023021002.
31. Liu H, Feng Y, Qian Z, Song Z, Zhang N, Yu J, Liu X, Qiu L, Zhou S, Gong W. Single-cell and bulk transcriptomics reveal a CD8+ T-cell gene signature predicting prognosis in diffuse large B-cell lymphoma. Front Immunol. 2025;16:1685541. doi: 10.3389/fimmu.2025.1685541.
32. Nam SJ, Go H, Paik JH, Kim TM, Heo DS, Kim CW, Jeon YK. An increase of M2 macrophages predicts poor prognosis in patients with diffuse large B-cell lymphoma treated with rituximab, cyclophosphamide, doxorubicin, vincristine and prednisone. Leuk Lymphoma. 2014;55(11):2466–2476. doi: 10.3109/10428194.2013.879713.
33. Ye X, Wang L, Nie M, Wang Y, Dong S, Ren W, Li G, Li ZM, Wu K, Pan-Hammarstrom Q. A single-cell Atlas of diffuse large B cell lymphoma. Cell Rep. 2022;39(3):110713. doi: 10.1016/j.celrep.2022.110713.
34. Liu M, Bertolazzi G, Sridhar S, Lee RX, Jaynes P, Mulder K, Syn N, Hoppe MM, Fan S, Peng Y, et al. Spatially-resolved transcriptomics reveal macrophage heterogeneity and prognostic significance in diffuse large B-cell lymphoma. Nat Commun. 2024;15(1):2113. doi: 10.1038/s41467-024-46220-z.
35. Luo M, Zhao F, Cheng H, Su M, Wang Y. Macrophage polarization: an important role in inflammatory diseases. Front Immunol. 2024;15:1352946. doi: 10.3389/fimmu.2024.1352946.
36. Herpin A, Lelong C, Favrel P. Transforming growth factor-beta-related proteins: an ancestral and widespread superfamily of cytokines in metazoans. Dev Comp Immunol. 2004;28(5):461–485. doi: 10.1016/j.dci.2003.09.007.
37. Bansod S, Doijad N, Godugu C. Berberine attenuates severity of chronic pancreatitis and fibrosis via AMPK-mediated inhibition of TGF-beta1/Smad signaling and M2 polarization. Toxicol Appl Pharmacol. 2020;403:115162. doi: 10.1016/j.taap.2020.115162.
38. Geng K, Ma X, Jiang Z, Gu J, Huang W, Wang W, Xu Y, Xu Y. WDR74 facilitates TGF-beta/Smad pathway activation to promote M2 macrophage polarization and diabetic foot ulcer wound healing in mice. Cell Biol Toxicol. 2023;39(4):1577–1591. doi: 10.1007/s10565-022-09748-8.
39. Liu Y, Chen X, Xu Y, Yang T, Wang H, Wang Z, Hu Z, Chen L, Zhang Z, Wu Y. CTHRC1 promotes colorectal cancer progression by recruiting tumor-associated macrophages via up-regulation of CCL15. J Mol Med (Berl). 2024;102(1):81–94. doi: 10.1007/s00109-023-02399-0.
40. Ribatti D, Tamma R, Annese T, Ingravallo G, Specchia G. Macrophages and angiogenesis in human lymphomas. Clin Exp Med. 2024;24(1):26. doi: 10.1007/s10238-023-01291-y.
41. Richards DM, Hettinger J, Feuerer M. Monocytes and macrophages in cancer: development and functions. Cancer Microenviron. 2013;6(2):179–191. doi: 10.1007/s12307-012-0123-x.
42. Gong H, Xue B, Ru J, Pei G, Li Y. Targeted therapy for EWS-FLI1 in ewing sarcoma. Cancers. 2023;15(16):4035. doi: 10.3390/cancers15164035.
43. Liu T, Xia L, Yao Y, Yan C, Fan Y, Gajendran B, Yang J, Li Y-J, Chen J, Filmus J. Identification of diterpenoid compounds that interfere with Fli-1 DNA binding to suppress leukemogenesis. Cell Death & Disease. 2019;10(2):117. doi: 10.1038/s41419-019-1363-1.
44. Shou M, Zhou H, Ma L. New advances in cancer therapy targeting TGF-β signaling pathways. Molecular Therapy-Oncolytics. 2023;31:100755. doi: 10.1016/j.omto.2023.100755.
45. Chen FZ, You LJ, Yang F, Wang LN, Guo XQ, Gao F, Hua C, Tan C, Fang L, Shan RQ, et al. CNGBdb: China national GeneBank DataBase. Yi Chuan. 2020;42(8):799–809.
46. Guo X, Chen F, Gao F, Li L, Liu K, You L, Hua C, Yang F, Liu W, Peng C, et al. CNSA: a data repository for archiving omics data. Database (Oxford). 2020;2020 baaa055. doi: 10.1093/database/baaa055.